



ELSEVIER

Contents lists available at ScienceDirect

Physica B

journal homepage: www.elsevier.com/locate/physb

Phase transformations in Mo-doped FINEMETs

Josefina M. Silveyra^{a,*}, Emília Illeková^b, Peter Švec^b, Dušan Janičkovič^b,
Andrés Rosales-Rivera^c, Victoria J. Cremaschi^{a,1}

^a Lab. de Sólidos Amorfos, INTECIN, FIUBA-CONICET, Paseo Colón 850, (C1063ACV) Buenos Aires, Argentina

^b Institute of Physics SAS, Dúbravská cesta 9, 845 11 Bratislava, Slovak Republic

^c Laboratorio de Magnetismo y Materiales Avanzados, Facultad de Ciencias Exactas y Naturales, Universidad Nacional de Colombia, Manizales, Colombia

ARTICLE INFO

Article history:

Received 5 March 2009

Received in revised form

23 March 2010

Accepted 24 March 2010

Keywords:

Phase transformations in amorphous alloys

Soft magnetic materials

FINEMET

ABSTRACT

In this paper, the phase transformations occurring during the crystallization process of FINEMETs in which Nb has been gradually replaced by Mo have been studied by a variety of techniques including DSC, DTA, TGA, XRD and TEM.

The thermal stability of the alloy was deteriorated as a consequence of Mo's smaller atomic size. The gradual replacement of Nb by Mo reduced the onset temperature of Fe–Si and of the borides. The Curie temperature of the amorphous phase slightly decreased from 594 K for $x=0$ to 587 K for $x=3$.

The borides compounds Fe_2B and Fe_{23}B_6 as well as the $(\text{Nb},\text{Mo})_5\text{Si}_3$ phase were found to precipitate in the second and third crystallization.

© 2010 Elsevier B.V. All rights reserved.

1. Introduction

Energy saving has become one of the main concerns in the last decades due to the increase in both lack of natural resources and global energy demand [1]. Research and development of magnetic materials that lower the energy loss is one way to tackle this issue. Following this trend a new kind of material with nanocrystalline structure [2] was developed in the last 30 years. These alloys exhibit excellent soft magnetic behaviour (high saturation flux density, very low coercivity and high permeability), which make them suitable for transformer cores. At the same time, the use of these materials reduces the CO_2 emission in the generating system, bringing an additional benefit: environment protection [3].

The discovery of these nanocrystalline materials opened a wide field in fundamental studies in solid state physics and, in particular, to understanding different phenomena related to the crystallization kinetics of magnetic amorphous alloys. The mechanisms involved in the transformation from the amorphous to the nanocrystalline state depend on diverse parameters like composition of the alloy, thermal history, diffusion coefficients of the different elements and concentration of the nucleation sites.

There is still disagreement among the researchers about the interpretation of FINEMET kinetics drawn from the unusual Avrami exponents that were obtained by different methods [4–7]. On the other hand, all of them agree on the role that Cu and Nb play in the crystallization. Cu atoms are not soluble in Fe

and increase the nucleation rate of the Fe–Si crystallites, favouring the nanocrystallization process. Nb atoms are preferentially located at the periphery of crystalline grains, playing a barrier-like role to the atomic diffusion, thus hindering the growth of the grains [8].

A partial substitution of 2% of Nb for Zr, Nb, Mo or V on the FINEMET alloy was carried out by Borrego and Conde [9] to study the effect of the refractory element in the devitrification transformation. In this work we present differential scanning calorimetry (DSC) and differential thermal analysis (DTA) results of crystalline ingots and amorphous ribbons of a new series of alloys where Nb was gradually replaced by Mo. Researchers [10–13] have reported a great increase in the permeability of this material when Nb was partially replaced by Mo. Thus, the aim of this work was to characterize thoroughly the phase transformations of the series. The study was complemented with thermogravimetric analysis (TGA) under a magnetic field and structural studies: X-ray diffraction (XRD) and transmission electron microscopy (TEM).

During the crystallization process of the FINEMET-type alloys different metastable phases appear, the identification of which has led to a large discrepancy among the different authors. Here, with the results obtained from diverse techniques we present a comprehensive study for the identification of the phases that appear in the devitrification of FINEMETs.

2. Materials and methods

FINEMET-type master alloys where Nb was substituted by Mo were prepared in an induction furnace ($\text{Fe}_{73.5}\text{Si}_{13.5}\text{B}_9\text{Nb}_{3-x}\text{Mo}_x\text{Cu}_1$

* Corresponding author. Tel.: +54 11 4343 9891x232; fax: +54 11 4331 1852.

E-mail address: jsilveyra@fi.uba.ar (J.M. Silveyra).

¹ CONICET member.

($x=0, 1.5, 2$ and 3) named from now on Mo0, Mo1.5, Mo2 and Mo3, respectively). Ribbons 10 mm wide and 20 μm thick were obtained from these ingots by the planar flow casting technique in air. The amorphous structure on both sides was checked by XRD and the chemical composition by inductively coupled plasma spectroscopy.

XRD was performed using a HZG 4 with graphite monochromator Cu $K_{\alpha 1}$ radiation.

DSC was performed using a Perkin–Elmer DSC7 under Ar flow of 30 ml/min at different heating rates (10, 20, 40 and 80 K/min) from 323 to 923 K. Temperature (± 1 K) as well as enthalpy ($\pm 5\%$) DSC instrument scales were calibrated with indium and zinc standards. DTA heating and cooling experiments were carried out in a Perkin–Elmer DTA7 instrument under Ar flux of 30 ml/min using the heating and cooling rates of ± 10 K/min within a temperature range from 323 to 1673 K. The standards used to calibrate the temperature (± 2 K) and the enthalpy (± 4 J/g) in the DTA instrument were aluminum and gold.

Continuous heating treatments with 10 K/min heating rate on samples used for TEM and XRD analyses were performed in vacuum up to the end of each transformation stage: (i) up to 868 K for all the samples, (ii) up to 980, 960, 958 and 940 K for Mo0, Mo1.5, Mo2 and Mo3, respectively and (iii) up to 1025 K for all the samples. The resulting phases were studied by XRD.

Mean grain size of traditionally annealed (813 K, 30 min) Mo0, Mo1, Mo1.5, Mo2 and Mo3 was determined by XRD and TEM. Conventional TEM was carried out in a JEOL-2000 FX microscope operating at 200 kV. TEM specimens were thinned by argon ion milling techniques.

TGA in a flowing N_2 atmosphere (10 ml/min for the scale and 90 ml/min for the furnace) in the presence of a small DC magnetic field produced by a weak magnet (3.5 G) was carried out in a TA Q500 thermobalance of TA Instruments to observe the thermal evolution. The measurements were performed at 10 K/min from room temperature up to 577 K and the device had been previously calibrated with nickel.

3. Results and discussion

FINEMET-type alloys change their structure and thermodynamic state when submitted to a continuous heating treatment. These transformations were studied by DSC (Fig. 1), DTA (Fig. 2) and TGA under a magnetic field (Fig. 3). Figs. 4, 5 and 6 show the comparison of DCS, DTA and TGA evolutions carried out at 10 K/min.

A structural relaxation (Relax) was seen in every metallic glass on DSC curves (inset, Fig. 1). Ribbons scanned at 40 K/min by DSC showed a structural rearrangement (R0) at around 750 K (inset Fig. 1) and is already described in [15]. It involved structural rearrangements that differ from those of conventional structural relaxation (Relax step); X-ray diffraction and transmission electron microscopy did not record any new crystalline phase at this step [15].

The first crystallization took place at higher temperatures (R1): nanocrystals of a non-stoichiometric Fe–Si DO3 structure (space group Fm3m) precipitated in the amorphous matrix (Fig. 7).

The shape of the DSC peak R1 did not change with Mo addition, so it is expected to maintain the same type of crystallization kinetics as traditional FINEMET [4] [17]. As previously explained, the kinetic parameters (diffusion coefficients and other factors) are composition-dependent and in this process the composition of the remnant amorphous phase changes during the crystallization of the Fe–Si: solute elements like B or Nb are rejected into the matrix [18]. These facts imply that the kinetics do not fit the conventional Johnson–Mehl–Avrami law [4–7]. R1 onset (T_{x1}) and

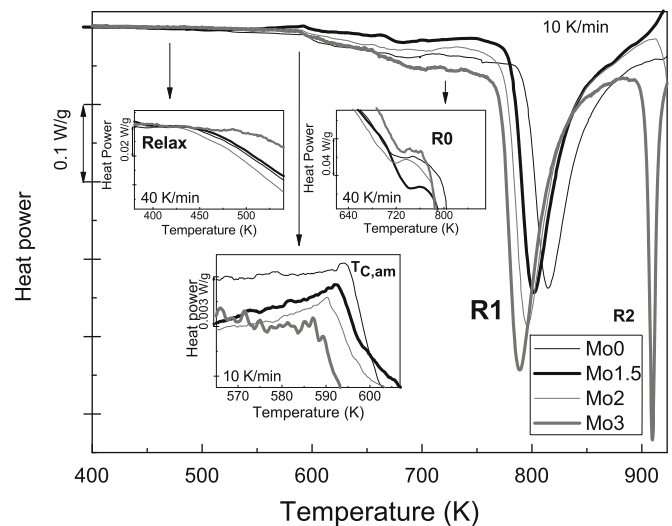


Fig. 1. DSC scans of as-quenched ribbons at 10 K/min. Insets: detail of Relax step (40 K/min), $T_{c,am}$ (10 K/min) and R0 step (40 K/min).

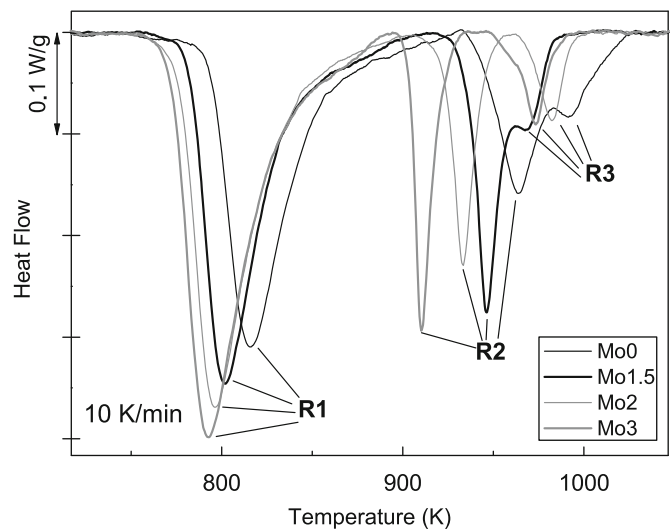


Fig. 2. DTA scans of the as-quenched ribbons (10 K/min).

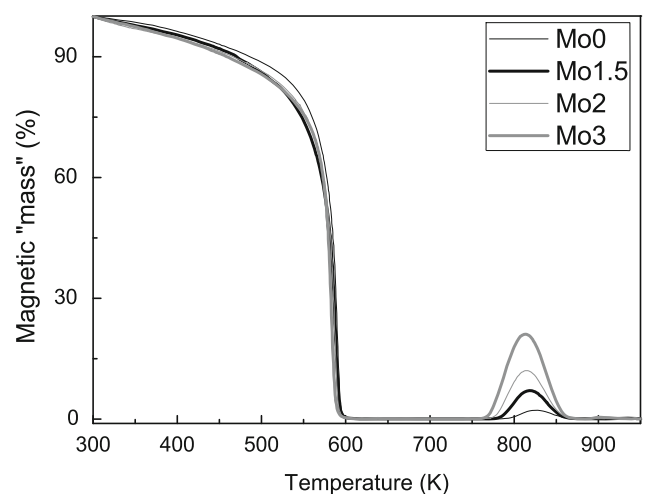


Fig. 3. TGA curves for Mo0, Mo1.5, Mo2 and Mo3 (10 K/min).

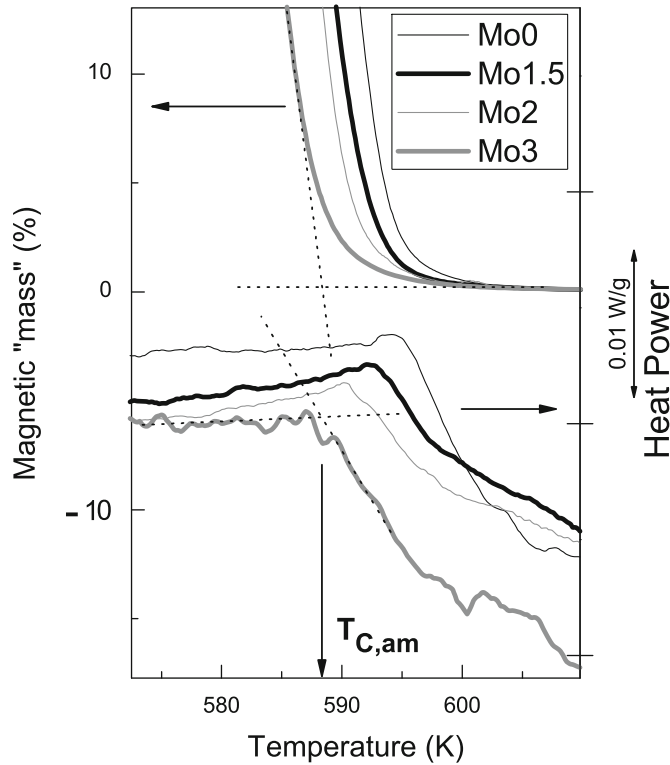


Fig. 4. TGA and DSC curves zoomed at $T_{C,am}$ (10 K/min). The dashed lines show the onset method used for determining $T_{C,am}$.

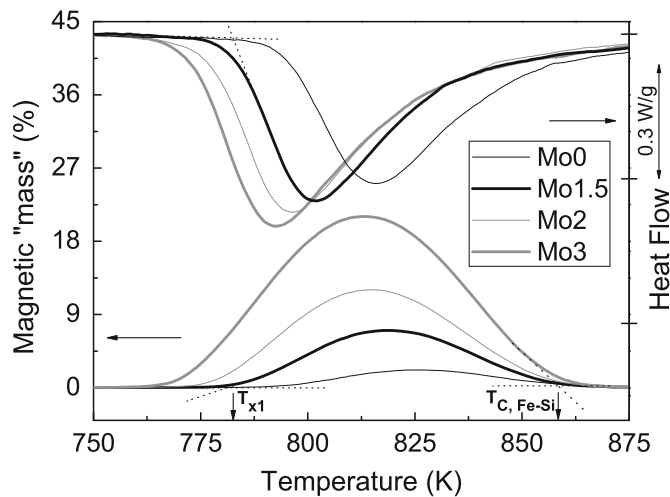


Fig. 5. TGA and DTA curves zoomed at R1 (Fe-Si crystallization) (10 K/min).

peak (T_{p1}) temperatures decreased with Mo content. The values obtained are presented in Table 1 for each alloy.

The Kissinger method [19] is based on the following equation:

$$\ln\left(\frac{\beta}{T_p^2}\right) = -\frac{E}{RT_p} + C \quad (1)$$

where β is the heating rate, T_p is the peak temperature, E the activation energy, R the universal gas constant and C a constant. According to Eq. (1), plots of $\ln(\beta/T_p^2)$ versus $1/T_p$ should result in straight lines, which slopes equal $-E/R$. Following this procedure, we obtained the activation energy of the primary crystallization (ΔE_1). This simple and well known method was used in order to compare the influence of the composition on ΔE_1 but not to focus on their absolute values [20]. The activation energy decreased

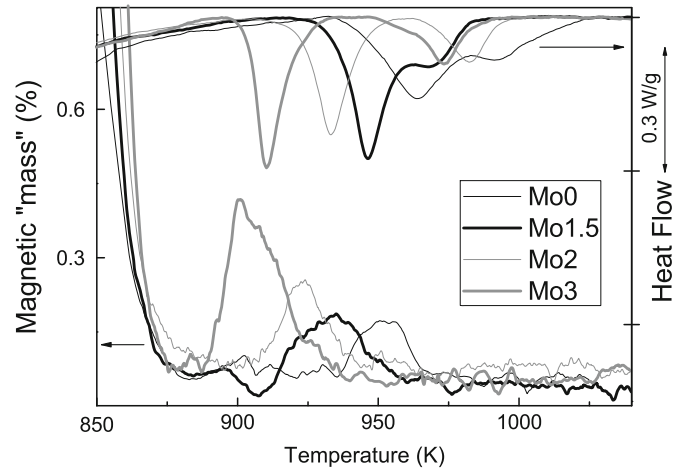


Fig. 6. TGA and DTA curves zoomed at R2 and R3 (Fe-B crystallization) (10 K/min).

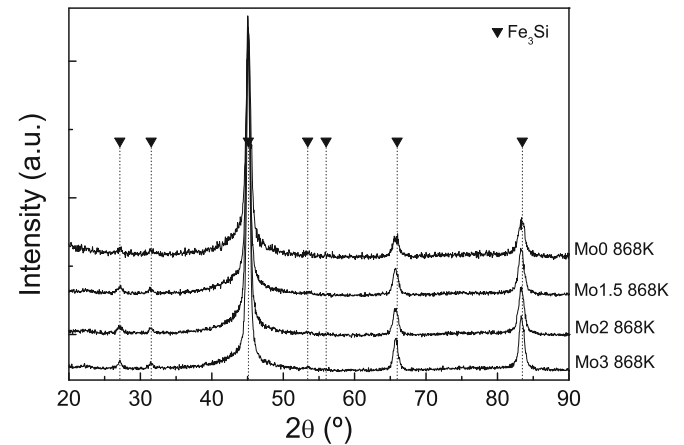


Fig. 7. X-ray diffractograms for Mo0, Mo1.5, Mo2 and Mo3 annealed at 10 K/min up to 868 K.

Table 1

Transformation temperatures: amorphous Curie temperature ($T_{C,am}$), relaxation temperature (T_{R0}), crystallization (T_x) and peak (T_p) temperatures.

Mo	$T_{C,am}$	T_{R0}	T_{x1}	T_{p1}	T_{x2}	T_{p2}	T_{p3}
K/min	10	40	10	10	10	10	10
0	594	772	794	815	899	962	991
1.5	592	758	782	802	917	946	968
2	590	749	778	796	926	933	980
3	587	741	772	789	937	910*	972

* This is the only T_{p2} that could be observed in DSC curves.

linearly with the replacement of Nb by Mo (Fig. 8) indicating that the crystallization of the Fe-Si phase was facilitated with the exchange.

The large atomic size of the refractory elements prevents the growth of Fe-Si grains during the nanocrystallization process. As Mo is smaller than Nb, it may be less effective in inhibiting the diffusion of Fe and Si atoms. This could explain why the substitution of Nb by Mo monotonously deteriorated the thermal stability of FINEMET alloy, i.e. the onset temperature was reduced. The smaller atomic size of Mo was probably responsible for the increase in the grains sizes in isothermally annealed samples, as observed by XRD and TEM. Mean grain size was estimated by the

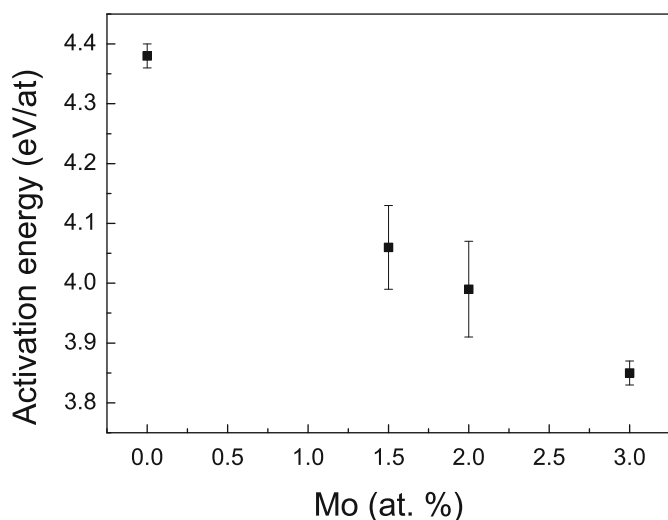


Fig. 8. Activation energy of the first crystallization peak (R1) calculated with the Kissinger method as a function of Mo content.

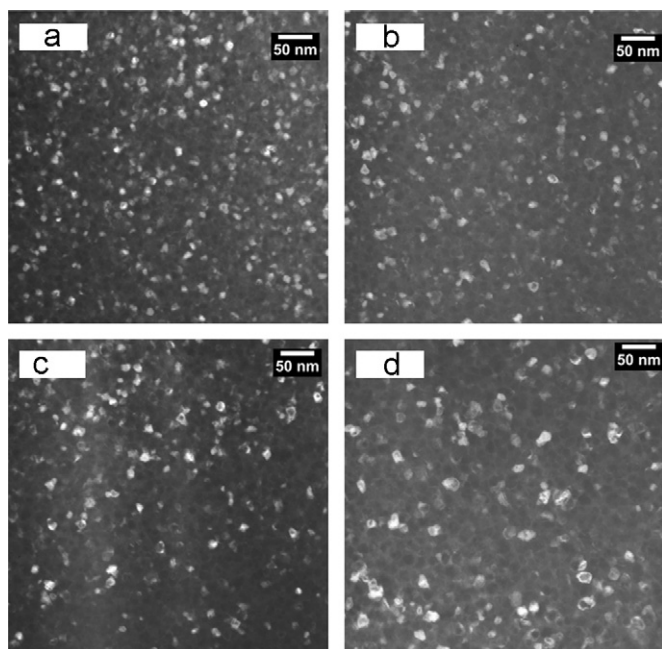


Fig. 9. Dark-field TEM images; (a) Mo0, (b) Mo1, (c) Mo2 and (d) Mo3.

Debye–Scherrer formula [21] and a direct relation between grain size and nominal Mo content was found: 11.9, 13.2, 15.1, 15.2 and 17.3 nm for Mo0, Mo1, Mo1.5, Mo2 and Mo3 annealed at 813 K during 30 min, respectively. Although this XRD method is prone to estimate larger values than the real ones, the same relative variation of mean grain size with the composition was observed with TEM (Fig. 9). The mean grain size (d) and standard deviation (SD) were estimated from the log-normal-distribution indicating the consistency of the results (d , SD): (9.1, 4.2), (9.4, 4.5), (11.2, 6.2) and (11.6, 5.7) nm for Mo0, Mo1, Mo2 and Mo3 annealed at 813 K during 30 min, respectively.

In TGA plots, the first fall in magnetization which corresponds to the transition from ferromagnetic to paramagnetic state was observed around 590 K (Fig. 3) for all the amorphous ribbons. This temperature, identified as the Curie temperature of the as-quenched amorphous phase ($T_{C,am}$), coincides perfectly well with the ones obtained by DSC measurements (Table 1, Fig. 4). $T_{C,am}$

was found to decrease with the replacement of Nb by Mo. The smaller size of Mo atoms (van der Waals radius: 0.139 nm) compared to those of Nb (0.143 nm) caused a decrease in the Fe–Fe interatomic distance. As it is known from the Bethe–Slater curve, lowering Fe–Fe interatomic distances decreases the exchange interaction among Fe atoms and therefore reduces the ferromagnetic behaviour of the material [14]. It is important to point out that the reduction in $T_{C,am}$ is not so unfavourable for these materials from the technological point of view, since it was less than 10 K when all Nb was substituted for Mo.

As the ferromagnetic Fe–Si crystalline phase has a Curie temperature higher than the crystallization one, R1 stage is also evidenced in TGA measurements where the sample exhibits an increase in magnetization (Fig. 5), corresponding to the onset of crystallization measured by DSC and DTA (T_{x1}). The difference between the magnetic “masses” obtained in TGA measurements from the different samples (see Fig. 5) might be explained as follows: Mo3 has the lowest T_{x1} and, therefore, will be the one with more Fe–Si crystalline fraction at a certain temperature. A larger Fe–Si crystalline fraction is the reason for the larger magnetic “mass”.

The ferro-paramagnetic transition of the crystalline phase is evidenced by a new fall to zero of the magnetization at $T_{C,Fe-Si} \sim 856$ K for all the samples (see Figs. 5 or 6). It is known that the Curie temperature of the stoichiometric Fe_3Si is 840 K, and for the compound with smaller Si content, i.e. $Fe_{3-x}Si_x$, it varies between 840 and 1043 K. Following the data of the Curie temperature as a function of Si content reported in Ref. [16], the Si content in the nanocrystals of our alloys should be around 20%.

Finally, two more exothermic steps were observed in DTA plots, R2 and R3 (Fig. 2). R3 was small and slightly overlapped with R2 in Mo0 and Mo1.5. This could be the reason why R3 was not identified until now on FINEMETs studies [17]. Peak temperatures, T_{p2} and T_{p3} , have been determined by DTA (Table 1) showing also a slight deterioration in thermal stability with the rare exception of $T_{p3|Mo1.5}$. R2 stage led to a new increase in the magnetization moment in the TGA curves (Fig. 6), indicating that an iron-containing phase precipitated. The onset temperature shift between DTA and TGA curves may be explained by the method used for calibrating of the TGA equipment (note that TGA was calibrated only with nickel which has a Curie temperature of 631 K).

By means of the X-ray diffractograms corresponding to the samples annealed up to the end of R2, two borides compounds were identified (Fig. 10): $Fe_{23}B_6$ and Fe_2B . Some small peaks identified as $(Nb,Mo)_5Si_3$ were also observed at this step, specially

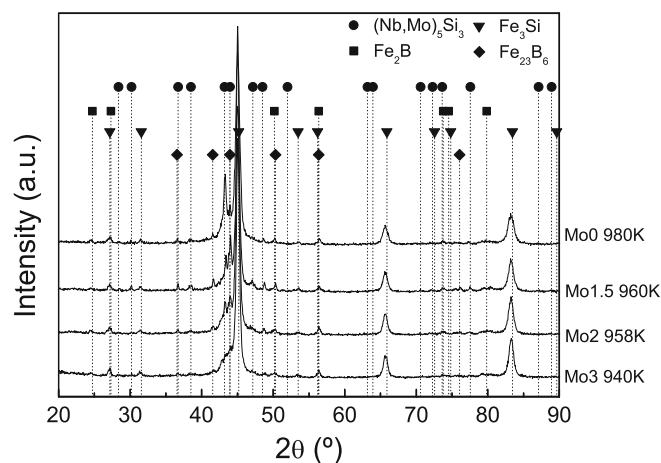


Fig. 10. X-ray diffractograms for Mo0, Mo1.5, Mo2 and Mo3 annealed at 10 K/min up to 980, 960, 958 and 940 K, respectively.

in Mo1.5. We suppose that this phase could actually belong to the R3 transformation but it was observed also on these annealed samples because R2 and R3 overlap with each other (see Fig. 6). The presence of the metastable phase Fe_3B , that is thought to decompose into Fe_{23}B_6 and Fe_2B [22], could not be dismissed since its possible peaks coincide with the ones of other phases. It could be assumed that the phases present are (Nb,Mo)-containing and that the refractory elements were incorporated in the phases by substituting Fe atoms. The shift of these peaks towards higher angles with Mo content in the samples indicates a decrease in the lattice parameter of the phases. The formation of substituted (Fe,Nb,Mo)-B clusters or regions in the amorphous phase [23,24] and compounds in crystallized samples [25–32] has been theoretically predicted and experimentally identified by several authors. The onset temperature of Fe–B peaks obtained from DTA curves (T_{x2}) decreased with Mo content. This behaviour may be explained analogously by the decrease in the onset temperature for the Fe–Si phase: smaller refractory elements are less effective in inhibiting the diffusion of B atoms as well.

The apparent increase on the magnetic “mass” magnetization visible in TGA at 875–975 K (see Fig. 6) should correspond to $(\text{Fe,Nb,Mo})_2\text{B}$ since the Curie temperature of this phase lies above its crystallization temperature T_{x2} ($T_{C,\text{Fe}2\text{B}} = 1015 \text{ K}$ [33]), while the Curie temperatures of the $(\text{Fe,Nb,Mo})_3\text{B}$ and $(\text{Fe,Nb,Mo})_{23}\text{B}_6$ phases are lower than the crystallization ones ($T_{C,\text{Fe}3\text{B}} \sim 800 \text{ K}$ [34] and $T_{C,\text{Fe}23\text{B}6} \sim 630 \text{ K}$ [35]). In fact, the $T_{C,\text{Fe}23\text{B}6}$ was pointed out for Mo0 and Mo2 in magnetization versus temperature curves of preheated samples in Fig. 5 of the work reported by Borrego and Conde [35]. As expected from our analysis, Mo2 showed a lower $T_{C,\text{Fe}23\text{B}6}$ value than Mo0, although no mention to this fact was made in their text. No evidence of presence of Fe_3B was found in their work either. The final decrease on the magnetic “mass” magnetization observed in TGA plots corresponds to the ferro-paramagnetic transition of $(\text{Fe,Nb,Mo})_2\text{B}$; a composition difference of this phase among the alloys might be responsible for the significant decrease of the borides’ Curie temperature with Mo content.

The XRD peaks corresponding to the $(\text{Nb,Mo})_5\text{Si}_3$ phase after R3 transformation are sharper and higher, due on the one hand, to the total disappearance of the remaining amorphous matrix at this high temperature and on the other hand, to the growth of this phase (Fig. 11). As we already stated, we assume that this phase precipitated at this stage (R3) but was also observed in some small XRD peaks belonging to R2 because of the difficulty of separating the overlapped transformations (Fig. 6) in the annealings. $(\text{Nb,Mo})_5\text{Si}_3$ phase was formed from some Si atoms

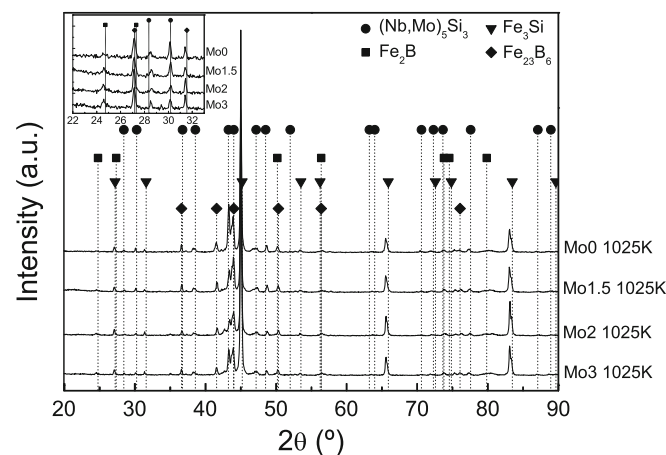


Fig. 11. X-ray diffractograms for Mo0, Mo1.5, Mo2 and Mo3 annealed at 10 K/min up to 1025 K.

that diffused out of Fe–Si grains, that is why Fe–Si XRD peaks shifted towards lower angles (Fig. 12). Furthermore, the decrease of the Fe–Si peaks width indicated the growth of the Fe–Si grains. Thus, this Fe–Si grain-growth together with $(\text{Nb,Mo})_5\text{Si}_3$ crystallization are attributed to R3 transformation in DTA runs. No new increase in magnetization was detected by TGA at this stage.

All mentioned transformation temperatures corresponding to Mo0, Mo1.5, Mo2 and Mo3 samples were tabulated in Table 1 for better comparison.

At higher temperatures ($> 1000 \text{ K}$), we compared the thermal stability of the ribbons and the master alloys using DTA. As an example there is a plot of Mo3 in Fig. 13 showing heating and cooling first and second runs. Some peak shape and size differences and shifts between ribbon and master alloy curves were observed. Nevertheless, the transformations were quite well reproduced.

Second run heating and cooling curves were found to be more homogeneous than the ones from the first run. This is more evident in the case of the ribbon since the sample was

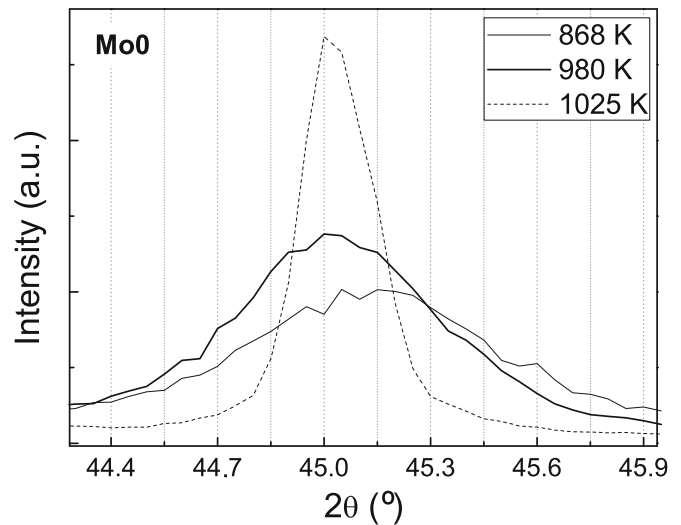


Fig. 12. XRD peak of Fe–Si [1 1 0] of the sample Mo0 annealed at 10 K/min up to 868, 980 and 1025 K.

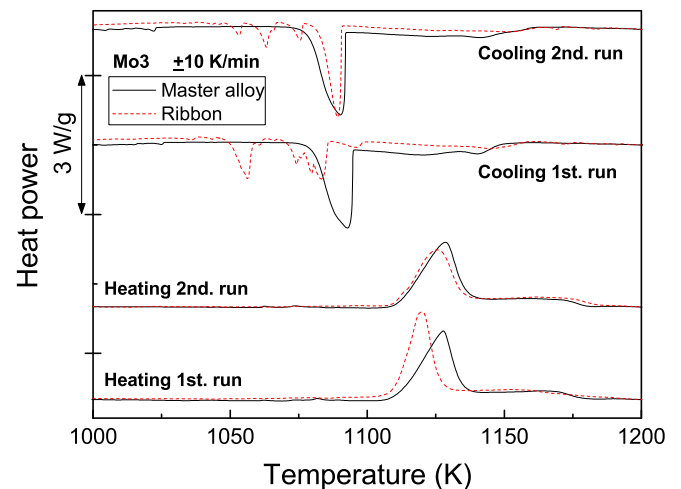


Fig. 13. DTA first and second scans of ribbon (dashed) and master alloy (continuous) (10 K/min).

composed of several small pieces instead of a single one as in the master alloy.

In the first heating run, the peaks slopes of the ribbon and the master alloy probably differ because on the difference in the thermal conductivity of the set of very thin strips in the case of the ribbon and a bulk piece in the case of the master alloy. In the second run, after the melting and reorganization into more similar phases, it can be seen how they are already more alike.

4. Conclusions

The thermal evolution of the FINEMET-type series $\text{Fe}_{73.5}\text{Si}_{13.5}\text{Nb}_{3-x}\text{Mo}_x\text{B}_9\text{Cu}_1$, $x=0, 1.5, 2, 3$ was studied by means of DSC, DTA, TGA, XRD and TEM. Because of the difference in atomic size between Mo and Nb, the substitution of Nb by Mo deteriorated monotonously the thermal stability of the FINEMET alloy:

- The shortening of Fe–Fe interatomic distances in amorphous samples led to a reduction of the exchange interaction among Fe atoms and therefore, to a slight monotonous decrease in $T_{C,am}$.
- As more Nb was replaced by Mo, the inhibition of the diffusion of Fe and Si atoms was systematically lower. That is why Fe–Si DO3 crystallization began at lower temperatures for continuous heating runs. For 813 K isothermal annealings, the mean grain size increased.
- The inhibition of B atoms' diffusion was systematically lowered as well, as evidenced in the earlier borides precipitation. The presence of Fe_2B was identified by TGA and XRD. XRD also confirmed the presence of Fe_{23}B_6 and the existence of Fe_3B could not be dismissed. The large and linear decrease of $T_{C,Fe-B}$ observed by TGA might be due to the differences in chemical compositions. Nb and Mo atoms present in these borides compounds were found to be substituting Fe atoms.

Acknowledgements

We thank Diego Coral for carrying out the TGA measurements and Juan Manuel Conde Garrido for the discussion of the results. This work was supported by the projects VEGA 2/0157/08, APVV-0413-06 and by the CEX “Nanosmart”.

References

- [1] F. Marechal, D. Favrat, E. Jochem, *Resour. Conserv. Recycling* 44 (2005) 245.
- [2] Y. Yoshizawa, S. Oguma, K. Yamauchi, *J. Appl. Phys.* 64 (1988) 6044.
- [3] I. Dincer, M.A. Rosen, *Appl. Energy* 64 (1999) 427.
- [4] E. Illeková, K. Czomorová, F.A. Kuhnast, J.M. Fiorani, *Mater. Sci. Eng. A205* (1996) 166.
- [5] G. Hampel, A. Pundt, J. Hesse, *J. Phys.: Condens. Matter* 4 (1992) 3195.
- [6] T. Pradell, D. Crespo, N. Clavaguera, M.T. Clavaguera-Mora, *J. Phys. Condens. Matter* 10 (1998) 3833.
- [7] J.M. Barandiarán, I. Tellería, J.S. Garitaonandía, H.A. Davies, *J. Non-Cryst. Solids* 329 (2003) 57.
- [8] N. Randrianantoandro, I. Labaye, L. Berger, O. Crisan, M. Grafoute, F. Calvayrac, J.M. Greneche, *J. Opt. Adv. Mater.* 4 (2) (2002) 193.
- [9] J.M. Borrego, A. Conde, *Mater. Sci. Eng. A* 226–228 (1997) 663.
- [10] V. Keylin, V.I.A. Belozarov, I.U.N. Starodubtsev, *Russian Patent # 2009257*, March 15, 1994, in Russian.
- [11] I.U.N. Starodubtsev, V. Keylin, V.I.A. Belozarov, B. Droschenko, S. Hlopunov, *Russian Patent # 2041282*, August 9, 1995, in Russian.
- [12] Y. Liu, G.Y. Liang, *Rare Met.* 21 (1997) 29, in Chinese.
- [13] I.U.N. Starodubtsev, V.I.A. Belozarov, *Magnetic properties of amorphous and nanocrystalline alloys*, Izd-vo Uralskogo Universiteta, 2002, 5-7525-1009-0, in Russian.
- [14] D. Muraca, J. Silveyra, M. Pagnola, V. Cremaschi, *J. Magn. Magn. Mater.* 321 (2009) 3640.
- [15] M. Miglierini, J. Degmová, T. Kaňuch, P. Švec, E. Illeková, D. Janičkovič, *Magnetic microstructure of amorphous/nanocrystalline FeMoCuB alloys*, in: B. Idzikowski, P. Švec, M. Miglierini (Eds.), *Properties and Applications of Nanocrystalline Alloys from Amorphous Precursors*, Kluwer Academic Publishers, 2004, p. 421.
- [16] L.K. Varga, F. Mazaleyrat, J. Kovac, J.M. Greneche, *J. Phys.: Condens. Matter* 14 (2002) 1985.
- [17] E. Illeková, *Thermochim. Acta* 387 (2002) 47.
- [18] J.M. Silveyra, J.A. Moya, V.J. Cremaschi, D. Janickovic, P. Švec, *Hyperfine Interact.* 195 (2010) 173.
- [19] H.E. Kissinger, *Anal. Chem.* 29 (1957) 1702.
- [20] M.J. Starink, *Thermochim. Acta* 404 (2003) 163.
- [21] H. Klug, L. Alexander, *X-Ray Diffraction Procedures*, Wiley, New York, 1954.
- [22] Y.R. Zhang, R.V. Ramanujan, *J. Alloys Compd.* 403 (2005) 197.
- [23] H. Hermann, N. Mattern, S. Roth, P. Uebele, *Phys. Rev. B* 56 (1997) 13888.
- [24] J. Sitek, J. Lipka, M. Miglierini, I. Toth, *J. Magn. Magn. Mater.* 140 (1995) 441.
- [25] M. Sarasola, T. Gómez-Acebo, F. Castro, *Acta Mater.* 52 (2004) 4615.
- [26] J.Z. Jiang, *Nanostruct. Mater.* 9 (1997) 245.
- [27] M. Imafuku, S. Sato, H. Koshiba, E. Matsubara, A. Inoue, *Scr. Mater.* 44 (2001) 2369.
- [28] M. Widom, M. Mihalkovic, *J. Mater. Res.* 20 (2005) 237.
- [29] J. Long, P.R. Ohodnicki, D.E. Laughlin, M.E. McHenry, T. Ohkubo, K. Hono, *J. Appl. Phys.* 101 (2007) 09N114.
- [30] R. Juhász, Á. Cziráki, L.F. Kiss, A. Lovas, *Mater. Sci. Eng. A* 375–377 (2004) 1057.
- [31] A. Hirata, Y. Hirotsu, E. Matsubara, *Intermetallics* 17 (2009) 796.
- [32] H. Hermann, N. Mattern, S. Roth, P. Uebele, *Phys. Rev. B* 56 (1997) 13888.
- [33] K.A. Murphy, N. Hershkowitz, *Phys. Rev. B* 7 (1973) 23.
- [34] C.L. Chien, D. Musser, E.M. Gyorgy, R.C. Sherwood, H.S. Chen, F.E. Luborsky, J.L. Walter, *Phys. Rev. B* 20 (1979) 283.
- [35] J.M. Borrego, C.F. Conde, A. Conde, *Philos. Mag. Lett.* 80 (2000) 359.